Synthesis of hyperbranched low molecular weight polyethylene oils by an iminopyridine nickel(II) catalyst†

Ilaria D'Auria, [a] Stefano Milione, [a] Tonino Caruso, [a] Gabriele Balducci [b] and Claudio Pellecchia *[a]

A 6-(2,6-dimethylphenyl)-2-(2,6-diisopropylphenyl)iminopyridine dibromo nickel(II) complex was synthesized, characterized by X-ray diffraction analysis and tested in ethylene polymerization using diethylaluminumchloride as the cocatalyst. Low molecular weight ($M_n \sim 10^3$ g mol^{-1}) polyethylene oils were obtained under a variety of reaction conditions. Detailed NMR analysis showed the formation of hyperbranched macromolecules (branching density >100 branches per 1000 carbons) with a high fraction of "branches on branch" and one unsaturation per chain, resulting in polymer features comparable to those of polymers produced by α-diimine Pd(II) catalysts. The DFT model of the catalytic species showed that the *ortho*-2,6-dimethylphenyl substituent of the pyridine group destabilizes the ethylene coordination to the metal centre but does not encumber both axial coordination site. So the polymerization performance of **1** can be addressed to the catalytic pocket generated by the coordinated ligand that favors both chain transfer and chain walking over propagation.

Accepted 2nd October 2017

Introduction

The breakthrough discovery of Ni(II) or Pd(II) α-diimine catalysts by Brookhart *et al.*[1] opened the era of *late-transition metal* olefin polymerization catalysts, spurring hundreds of studies by researchers from both academia and industry over the last twenty years.[2–7] The unique ability of the Brookhart catalysts to promote a "chain-walking" mechanism of polymerization, a process involving a number of β-hydride eliminations and reinsertions with opposite regiochemistry, results in the production of macromolecules with a variable content of branches of different lengths, affording polymers ranging from semicrystalline plastics to thermoplastic elastomers to hyperbranched amorphous waxes and oils. For Ni catalysts, the degree of branching was shown[1–7] to depend on temperature, monomer pressure and catalyst structure: higher branching is favored by higher polymerization temperature, lower monomer pressure and larger steric bulk in the axial positions of the square-planar coordination sphere; the latter feature is also required for the achievement of high molecular weight polymers. A mechanism involving a cationic 16-electron β-agostic Ni(II) complex as the resting catalyst state (in equilibrium with the alkyl ethylene complex), for which the relative rates of chain-walking and monomer trapping are affected by temperature, pressure and the steric hindrance of the ligand, clearly explained the above findings.[1–9] For α-diimine Pd(II) catalysts, on the other hand, the resting state is the Pd(II) ethylene π-complex and, as a consequence, hyperbranched polyethylenes (*i.e.* containing "branch-on-branch structures", HBPE) are produced, with branching densities substantially independent on monomer pressure (which however affects the polymer topology[10,11]) and reaction temperature.[1–9]

Low molecular weight polyethylenes and ethylene unsaturated oligomers can be also obtained using less bulky diimine ligands: Ni(II) catalysts yield linear unsaturated oligomers with high activity, while Pd(II) catalysts produce branched oligomers with low activities.[2–7,12,13] Highly branched low-molecular weight polyethylenes or oligoethylenes are of interest as, *e.g.*, additives in polymer blendings, in lubricants or in surface modifiers.[13–16] As stated in a recent review,[14] "the commercial applications of HBPE materials are currently restricted primarily due to the high cost, low activity and stability of the existing Pd–diimine catalysts. The discovery of new, highly active, and cost-effective catalysts (for example, the Ni-based catalysts) with competing performance features thus remains the major challenge in the area". Actually, some significant advances in

[a]*Dipartimento di Chimica e Biologia "A. Zambelli", Università di Salerno, via Giovanni Paolo II 132, I-84084 Fisciano, SA, Italy. E-mail: cpellecchia@unisa.it*

[b]*Dipartimento di Scienze Chimiche e Farmaceutiche, Università di Trieste, Via Giorgieri 1, I-34127 Trieste, Italy*

this direction have been recently reported. For example, Mecking *et al.* reported that neutral salicylaldiminato Ni(II) catalysts bearing *N*-terphenyl groups with CH_3 substituents on the peripheral aromatic rings (Chart 1, **A**) yield hyperbranched ethylene oligomers with M_n *ca.* 10^3 g mol^{-1}, while the corresponding CF_3-substituted catalyst produced semicrystalline polyethylene with low branching, pointing to a remote ligand electronic effect.[17,18] Marks *et al.* reported the production of hyperbranched oligoethylenes, having even higher branching densities, by salicylaldiminato Ni(II) catalysts bearing a hemilabile $-SO_2Ph$ moiety, in contrast to the analogous catalyst displaying a $-CH_2Ph$ dangling group (Chart 1, **B**), suggesting a structure modulation by coordination of the SO_2-Ph group.[19] Brookhart, Daugulis *et al.* showed that Ni(II) α-diimine catalysts incorporating 8-*p*-tolylnaphtylimino groups (Chart 1, **C**) yield more branched polyethylenes than standard Brookhart catalysts bearing 2,6-isopropylphenylimino moieties, owing to the increased axial bulk.[20]

Early studies by the group of Laine[21–23] showed that nickel(II) catalysts bearing iminopyridine ligands with 2,6-alkylphenyl substituents on the imino moiety and no substituent in the 6-position of the pyridine moiety produce nearly linear or moderately methyl branched low molecular weight polyethylenes, depending on the reaction temperature.[21] Introduction of a methyl substituent in the 6-position of pyridine resulted in the production of even more linear polyethylenes with slightly higher molecular weight and decreased activity.[23] On the other hand, Kempe *et al.*[24] reported that nickel(II) dichloride complexes bearing similar ligands having a 2,6-dialkylphenyl substituent in the 6-position of pyridine (alkyl = Me, or i-Pr), activated by MAO, promote prevailingly ethylene dimerization to 1-butene with minor amounts of C6, C8 and higher oligomers.

More recently, Sun *et al.* reported iminopyridine Ni(II) catalysts containing *o*-benzhydryl substituents on the arylimino moiety of the ligand, but no substituents on the pyridine moiety, resulting in the production of low molecular weight moderately branched polyethylenes with high activities.[25–27] Subsequently, Brookhart, Daugulis *et al.* have shown that Ni complexes bearing iminopyridine ligands incorporating very bulky 8-arylnaphtyl substituents on the imino moiety, blocking only *one* of the two coordination sites at the metal centre, yield moderately branched polyethylenes with increased molecular weight (~10^4 g mol^{-1}).[28]

We report here that hyperbranched low molecular weight ($M_n \sim 10^3$ g mol^{-1}) polyethylene oils can be produced by a Ni(II) dibromo complex bearing the sterically encumbered iminopyridine ligand 6-(2,6-dimethylphenyl)-2-(2,6-diisopropylphenyl)iminopyridine (**L1**, see Scheme 1) after activation with diethylaluminumchloride ($AlEt_2Cl$).

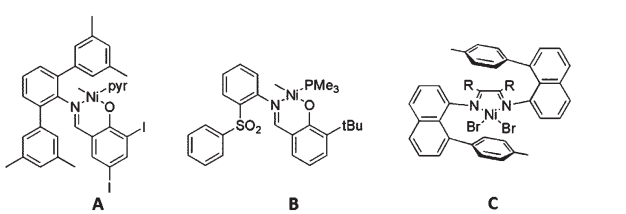

A B C

Chart 1

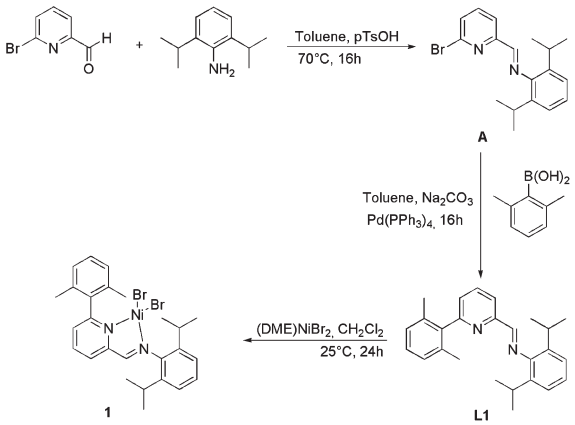

Scheme 1 Synthetic procedure for ligand **L1** and Ni complex **1**.

Results and discussion

Synthesis and X-ray structure of the Ni complex

The ligand **L1** was synthesized in two steps by condensation reaction of 6-bromo-2-pyridinecarboxyaldehyde and 2,6-diisopropylaniline, followed by Suzuki coupling of the resulting 6-bromo-2-(2,6-diisopropylphenyl)iminopyridine and 2,6-dimethyl-1-phenylboronic acid (yield 47%) (Scheme 1). During the course of our study, we realized that the same ligand had been previously prepared using a different reaction pathway, involving condensation of 6-bromo-2-pyridinecarboxyaldehyde and 2,6-diisopropylaniline, followed by Kumada coupling with the Grignard compound 2,6-dimethylphenyl magnesium bromide.[24] Nickel complex **1** was synthesized in 86% yield by reaction of (dimethoxyethane)nickel dibromide and a slight excess of **L1** in methylene chloride.

Complex **1** was characterized by HR ESI FT-ICR Mass Spectroscopy [(L1–Ni–Br)$^+$ *m*/*z* 507.0940] (see the Experimental section and Fig. S4†) and single crystal X-ray diffraction analysis. Single crystals of yellow paramagnetic complex **1** were grown from a methylene chloride solution by slow diffusion of layered *n*-hexane at room temperature. In the crystal structure of **1** (which contains one molecule of chlatrated CH_2Cl_2, disordered over three distinct positions, see Fig. 1 and the Experimental section) the Ni atom displays a distorted tetrahedral coordination, where the N1–Ni1–N2 angle is forced to the low value of 82°, being included in a rigid five membered chelate ring. While the Ni–N bond lenghts are identical, the Ni–Br2 distance is slightly longer than the Ni–Br1 one; consistently, the Br2–Ni–N1 and Br2–Ni–N2 coordination angles are smaller than the corresponding quantities for the Br1 ligand; on the other hand, the Br2–Ni–Br1 and N1–Ni–N2 planes are almost perfectly perpendicular (dihedral angle: 89.49°). Due to

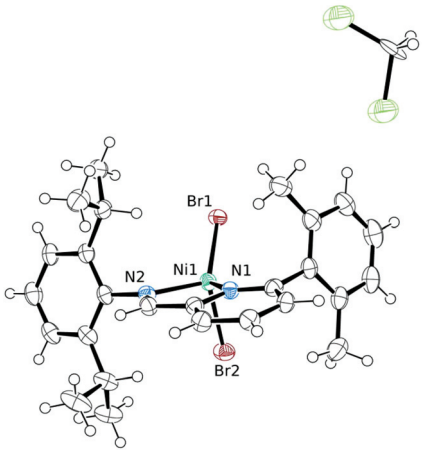

Fig. 1 ORTEP representation of the crystal structure of complex **1** (thermal ellipsoids at 50% probability level); for clarity, only the most populated CH_2Cl_2 solvent molecule has been included in the figure.

the presence of the isopropyl and methyl groups in *ortho* position, both phenyl rings adopt an orientation almost perpendicular to the plane of the bidentate ligand in order to minimize steric hindrance. Tetrahedral distortion, coordination bond lengths and angles are similar to those found in comparable structures reported in the literature.[29,30]

Polymerization of ethylene and polymer characterization

Complex **1** was tested in the polymerization of ethylene after activation with diethylaluminum chloride[31] ($AlEt_2Cl$) under a variety of conditions of temperature and monomer pressure. The polymerization conditions and results of some representative runs are displayed in Table 1 and in Table 2.

Some polymerization runs were initially carried out at 20 °C and 1 atm monomer pressure, preparing the catalyst/cocatalyst mixture in ethylene atmosphere. No solid polymer was produced, but GC-MS analysis of the reaction mixtures revealed the presence of oligomers in the range C4–C8 and higher (*v. infra*). Extraction of the reaction mixtures with hexane and solvent removal under reduced pressure resulted in the isolation of oily materials that were characterized as hyperbranched low molecular weight polyethylenes by ^1H and ^{13}C NMR analysis (*v. infra*). A 4×10^{-4} M concentration of Ni catalyst and an $AlEt_2Cl$/**1** ratio = 200 were selected as convenient conditions: an increase of the Al/Ni ratio to 400 resulted in a lower yield (*cf.* runs 1 and 3, Table 1), possibly owing to catalyst degradation, as suggested by the change of the reaction mixture colour from orange to green. The same green colour was observed when the catalyst-cocatalyst mixture was prepared in the absence of ethylene, resulting in significantly lower polymer productivities. The catalyst species seems sluggish but stable under the above conditions, since the productivity increases with reaction time over several hours (*cf.* runs 1, 5 and 6, Table 1). Use of MAO instead of $AlEt_2Cl$ under the same conditions resulted in a lower yield (*cf.* runs 1 and 4, Table 1). Use of a lower reaction temperature (0 °C, run 7, Table 1) also resulted in a lower yield, while at 50 °C (run 8, Table 1) the yield is only slightly decreased, reasonably due to the lower monomer concentration (*v. infra*).

Some runs were then carried out in autoclave at increasing monomer pressure, resulting in the production of multigram quantities of low molecular weight polyethylene oils. The catalyst productivity is roughly proportional to the monomer pressure at constant temperature (*cf.* run 5 of Table 1 and runs 9, 11, 12 and 13 of Table 2), at variance with the Brookhart's

Table 2 Polymerization of ethylene in autoclave at higher monomer pressure[a]

Run	T (°C)	P (atm)	Time (h)	Yield (g)	$M_n \times 10^{-3}$ (NMR)[b]	$M_n \times 10^{-3}$ (GPC)[c]	PDI (GPC)[c]
9	20	5	4	1.6	1.0	1.4	1.9
10	40	5	4	1.9	1.0	1.5	1.7
11	20	15	4	4.5	1.2	1.6	1.9
12	20	25	4	6.0	1.3	1.7	1.9
13	20	45	4	6.8[d]	1.0	1.4	1.9
14	50	50	4	5.5	0.7	1.0	1.8

[a] Conditions: Ni catalyst 10 μmol; cocatalyst, $AlEt_2Cl$ = 2.0 mmol; solvent, toluene = 50 mL. [b] Calculated from ratio between total resonance integral and unsaturated end group intensity in the ^1H NMR. [c] In THF *vs.* polystyrene standards. [d] Traces of solid polymer were also produced.

Table 1 Polymerization of ethylene at 1 atm monomer pressure[a]

Run	T (°C)	Cocatalyst (mmol)	Time (h)	Yield (g)	$M_n \times 10^{-3}$ (NMR)[b]	$M_n \times 10^{-3}$ (GPC)[c]	PDI (GPC)[c]
1	20	$AlEt_2Cl$ (2.0)	2	0.18	1.1	1.3	1.7
2	20	$AlEt_2Cl$ (1.0)	2	0.16	1.1	1.6	1.7
3	20	$AlEt_2Cl$ (4.0)	2	0.10	1.2	1.3	2.0
4	20	MAO (2.0)	2	0.11	1.2	1.2	2.0
5	20	$AlEt_2Cl$ (2.0)	4	0.31	1.1	1.4	1.8
6	20	$AlEt_2Cl$ (2.0)	16	0.48	1.1	1.3	1.8
7	0	$AlEt_2Cl$ (2.0)	2	0.10	1.5	1.8	1.8
8	50	$AlEt_2Cl$ (2.0)	2	0.15	0.5	0.7	1.6

[a] Conditions: Ni catalyst 10 μmol; solvent, toluene = 25 mL, ethylene pressure = 1 atm. [b] Calculated from ratio between total resonance integral and unsaturated end group intensity in the ^1H NMR. [c] In THF *vs.* polystyrene standards.

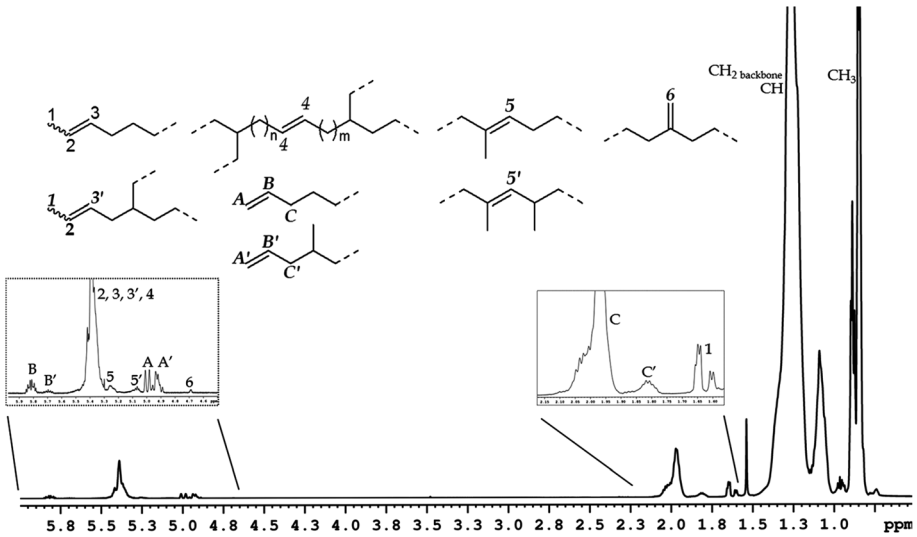

Fig. 2 ^{1}H NMR spectrum ($CDCl_3$) of a typical low molecular weight hyperbranched polyethylene sample. Resonances of the unsaturated protons are assigned according to ref. 13 and 18.

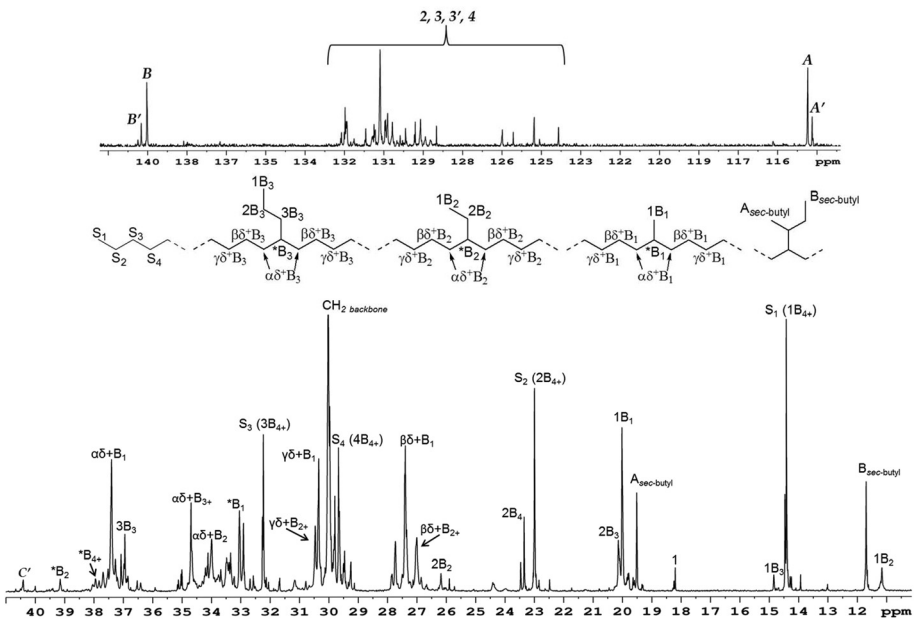

Fig. 3 Unsaturated (top) and aliphatic (bottom) region of the ^{13}C NMR spectrum ($CDCl_3$) of a typical low molecular weight hyperbranched polyethylene sample. Resonances are assigned according to ref. 13, 18, 32 and 33. Unsaturated and end groups carbons are numbered according to the schemes of Fig. 2.

α-diimine Pd(II) catalysts, for which a zero order kinetic in monomer concentration was observed.[2] The substantial insensitivity of the latter catalysts to the reaction conditions and in particular to the monomer pressure was an obvious limitation for practical applications.

The microstructures of the polymer samples were established by ^{1}H and ^{13}C NMR analysis: typical ^{1}H and ^{13}C NMR spectra are displayed in Fig. 2 and 3, where representative resonances diagnostic of branches of different lengths, assigned according to the literature,[32,33] are evidenced. The relative amount of the different branches are reported in Table 3 for all the samples of Tables 1 and 2.‡

‡For polyethylenes having molecular weights of the order of 10^3 g mol^{-1} (*i.e.* containing ≈70 ÷ 100 carbons per chain), use of the "number of branches per 1000 carbons" to express the degree of branching is questionable, but we used it for a better comparison with literature data. It is also worth mentioning that for such low molecular weight polymers both the overall degree of branching and the amount of "long chain branches" (*i.e.* branches of 4 carbons or longer) must be evaluated subtracting the contribution of chain ends.[18,34]

Table 3 Distribution of different branches by ^{13}C NMR analysis

Run	Total branches[a]	Methyl[b] (%)	Ethyl[b] (%)	Propyl[b] (%)	LCB[c] (%)	*sec*-Butyl[b] (%)
1	114	65.9	6.5	2.1	12.6	12.9
2	111	62.5	5.1	1.8	19.4	11.2
3	92	63.9	6.6	2.1	15.0	11.3
4	128	70.5	6.0	1.8	10.4	11.2
5	110	61.8	6.0	2.1	17.7	12.3
6	115	63.4	6.4	2.4	14.3	13.4
7	113	76.3	5.2	1.9	7.5	9.1
8	90	62.0	7.7	3.2	14.4	16.9
9	112	76.0	5.1	2.1	7.9	8.8
10	104	68.7	5.5	1.9	14.0	9.8
11	114	80.4	4.8	2.1	5.5	7.1
12	120	83.7	3.8	2.0	3.8	6.5
13	101	84.0	3.6	2.4	3.8	6.1
14	90	76.3	5.3	2.2	4.5	11.8

[a] Branches per 1000 carbons‡ calculated from ^1H NMR. [b] Calculated by the relative intensities of the methyl resonances $1B_1$, $1B_2$, $1B_3$, and $1B_2$-*sec*-Bu. [c] LCB = butyl and longer branches, calculated by the relative intensity of the methine resonance of the *br*-B_{4+}, since the main contribution to the integral of the methyl resonance $1B_{4+}$ is due to the chain end groups.[18]

For all the samples, one unsaturation per macromolecule is present, as expected for chain termination occurring *via* β-hydride transfer and as observed for similar low molecular weight polyethylenes obtained by other Ni and Pd catalysts.[12,13,18,34] Experimental evidence of the formation of prevailingly mono-unsaturated macromolecules comes from (i) the substantial agreement between the M_n calculated from the ^1H NMR spectra (from the ratio between total resonance integral and unsaturated methylene and methine intensities) and the M_n measured by GPC (see Tables 1 and 2); and (ii) from the ^{13}C NMR spectra, where the integral intensities of the methylene carbons of the saturated end groups (S2 and S3 in Fig. 3) are *ca.* one half of the total intensity of the unsaturated methylene and methine carbons. Owing to extensive chain walking, internal vinylene groups are the major unsaturations (>80%): only ~10% of the latter are 2-butenyl end groups, as indicated by the relative intensities of the CH_3–CH=CH··· resonance and of the ···CH=CH··· resonances (see Fig. 2). Allyl CH_2=CH–CH_2··· end groups are the second most abundant unsaturations (~15%), while internal methyl substituted double bonds and vinylidene groups are below 5%.[13,18]

The formation of hyperbranched low molecular weight polyethylenes is indicated by the presence of branch-on-branch structures, as clearly evidenced by the intense resonances of *sec*-butyl groups (*v. infra*). Overall, the structure of the macromolecules is similar to that of the oligoethylenes obtained by Mecking using *N*-terphenyl substituted salicylaldiminato Ni(II) catalysts,[18] but in our samples the branching density is higher (>100 branches per 1000 C's), comparable to that of the low molecular weight hyperbranched polyethylenes produced by α-diimine Pd(II) catalysts.[13]

The molecular weights evaluated from ^1H NMR are of the order of 10^3 g mol^{-1}, while the values obtained by GPC *vs.* linear polystyrene standards are slightly higher, as previously observed for similar branched polyethylenes.[18] Molecular weight distributions are very narrow, with PDI below 2.

The polymer features are only slightly affected by the reaction conditions in the explored range: the molecular weight decreases while the temperature increases (*cf.* runs 1, 7 and 8, Table 1), but it is substantially unaffected by the monomer pressure. The total number of branching is also poorly sensitive to variation of the reaction temperature and pressure. As previously observed in the case of α-diimine Pd(II) catalysts,[10,11] the fraction of branch-on-branch structures is affected by the monomer pressure: in fact, the content of *sec*-butyl branches is 12.9% for a sample prepared at 20 °C and 1 atm (run 1, Table 1), but it is only 6.1% for a sample prepared at 20 °C and 45 atm (run 13, Table 2). Interestingly, in all samples >60% of all ethyl branches are present in *sec*-butyl groups, which is a higher fraction than that observed in the hyperbranched polyethylenes produced by α-diimine Pd(II) catalysts.[2,10,11,13] The mechanism of formation of *sec*-butyl branches proposed by Brookhart *et al.*[2] involves metal migration at a tertiary carbon atom followed by subsequent migration back down the chain (Scheme 2a); on the contrary, an ethyl branch is produced if the catalyst, after migration at the tertiary carbon, migrates to the primary carbon (Scheme 2b). Route of Scheme 2a seems highly favoured *vs.* path 2b in our catalyst system, considering that ethyl branches can derive also from two consecutive chain walkings not involving tertiary carbons.

The production of the above described hyperbranched oligoethylenes by iminopyridine catalyst **1** is in some way unexpected: according to the literature,[1–9,20] increasing steric bulk in the axial positions of *both* coordination sites of the square planar Ni(II) active species results in the production of polyethylenes having *both* higher molecular weight and more branches. In fact, in Brookhart's mechanistic scheme[1,2,8,9] increase of steric bulk leads to an increase of the ground state energy of the resting state and consequently to a decrease of the barrier to migratory insertion. Increasing steric bulk also increases the barrier to chain transfer either *via* β-hydride elimination or transfer to the monomer.

On the other hand, as mentioned in the introduction, a catalyst system based on a complex very similar to **1** and MAO was previously reported to promote prevailingly ethylene dimerization to 1-butene with minor amounts of C6, C8 and higher oligomers.[24] In order to quantify the amount of volatile oligomers produced by **1**-$AlEt_2Cl$ in our conditions, aliquotes

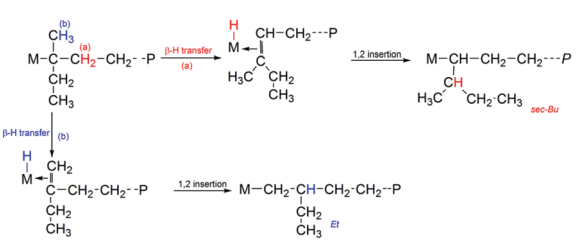

Scheme 2 Mechanism of formation of *sec*-butyl *vs.* ethyl branches.

Table 4 GC quantitative analysis of volatile unsaturated oligomers for selected runs

Run	C4 (g)	C6 (g)	C8 (g)
7	<0.01	<0.01	<0.01
9	0.04	0.01	0.01
11	0.30	0.02	0.02
12	0.55	0.03	0.03
13	0.70	0.04	0.04
14	0.31	0.04	0.03

of the reaction mixtures of selected runs were analysed by quantitative GC-MS (see Table 4 and the Experimental section for details). For all the samples, the amounts of C4–C8 olefins (mainly butenes) are significantly lower (at most 10%) than the amount of the oily low molecular weight fractions isolated from the reaction mixtures. The different results reported by Kempe *et al.*[24] are possibly due to the different conditions used in their study (the Ni precatalyst was a Ni dichloride complex, having a significantly lower concentration, the co-catalyst was MAO). Moreover, ref. 24 reports GC analysis of the volatile products, but extraction of the reaction mixtures and subsequent solvent distillation to look for soluble higher MW oligomers/polymers was not mentioned.

DFT calculations

With the aim to obtain better insight into the mechanism leading to the production of the hyperbranched oligoethylenes by **1**-$AlEt_2Cl$ catalytic system, the elementary steps involved in the polymerization reaction, *i.e.* chain propagation, termination and chain isomerization, were investigated by DFT methods using the cationic *n*-propyl derivative of **1** as the model complex of the active species. For the latter, two different isomers exist, depending on the position of the alkyl group, which can be either *trans* to the imine nitrogen or *trans* to the pyridine nitrogen. Hereinafter, we will refer to them by adding the *-im* or *-py* suffixes to the numbering of the structures we discuss. Also, since the coordination sites are not equivalent, two distinct reaction pathways (hereinafter referred to as the "imine" reaction path and the "pyridine" reaction path) can be identified, depending on the isomeric initiating alkyl complex.

Chain propagation. The Gibbs free energy profiles for chain propagation are depicted in Fig. 4 (green paths). The calculations start from the β-agostic *n*-propyl Ni cations. The isomer featuring the alkyl group *trans* to the pyridine group (**0-py**) is more stable by 4.1 kcal mol^{-1} than the other one with the alkyl group located in position *trans* to the imine group (**0-im**). The coordination of ethylene is only slightly exothermic for both isomers, in particular the enthalpy gain is −4.4 and −3.7 kcal mol^{-1} from **0-im** and **0-py**, respectively. As a consequence of the reduction of entropy associated with monomer coordination, an increase of free energy is obtained. The $-T\Delta S$ contribution to the free energy variation is about 11 kcal mol^{-1}; that is close to the value calculated (at 298 K) for olefin coordination to the Brookhart's Ni(II) diimine catalyst.[35]

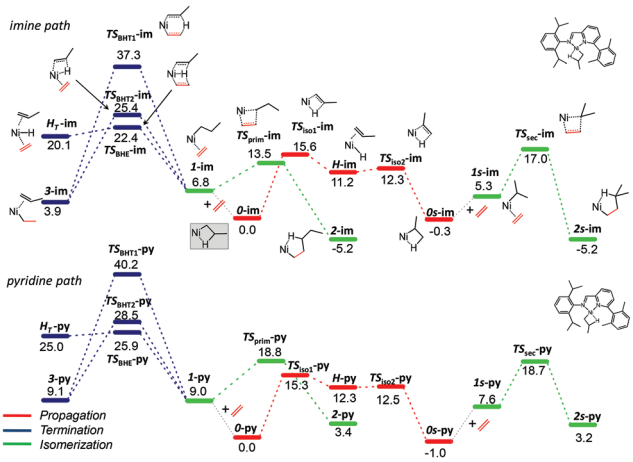

Fig. 4 Relative Gibbs free energy profiles corresponding to the competitive reactions for 6-(2,6-dimethylphenyl)-2-(2,6-diisopropylphenyl) iminopyridine Ni(II) complex **1**. Energies are given in kcal mol^{-1}.

In order to address the influence of the *ortho*-2,6-dimethylphenyl substituent of the pyridine group, we also modelled the reaction catalysed by the nickel(II) complex featuring the ligand lacking the substituent at the pyridine moiety, *i.e.* 2-(2,6-diisopropylphenyl)iminopyridine (**L2**).[36] The corresponding Gibbs free energy profiles are reported in Fig. S1 of the ESI.† In the latter case, the energy gain for ethylene coordination is higher, the enthalpy variation is −8.9 kcal mol^{-1} for both isomers. Thus, the presence of the *ortho*-2,6-dimethylphenyl group on the pyridine ring results in destabilization of the olefin π-complex.

In the π-complexes **1-im** and **1-py**, the double bond of the coordinated ethylene is nearly perpendicular to the Ni–C_α bond of the growing chain, while the C_β atom is pushed out of the imine–pyridine ring plane. The barrier to ethylene insertion into the Ni–C bond is 6.7 kcal mol^{-1} starting from **1-im**, and 9.8 kcal mol^{-1} starting from or **1-py** (see Fig. 4). The insertion leads to the γ-agostic-Ni-pentyl species **2-py** or **2-im**, that lie 12.0 kcal mol^{-1} or 5.6 kcal mol^{-1} below the complexes **1-im** and **1-py**, respectively. The structures of the transition states for the imine path are displayed in Fig. 5. These data suggest that the propagation through the "imine" reaction path is more favoured.

The increase of the steric bulk of the alkyl chain bound to the nickel centre does not destabilize the complexes: actually, the β-agostic Ni-isopropyl cations and the corresponding π-olefin complexes are slightly more stable than the analogous Ni complexes bearing the *n*-propyl chain (*e.g.* compare ***0-py*** *vs.* ***0s-py*** or ***1-py*** *vs.* ***1s-py***). Also, ethylene coordination is not hampered by the isopropyl chain. The steric hindrance of the isopropyl chain, however, affects the activation barriers for ethylene insertion in the secondary Ni-alkyl bond: they are 11.7 kcal mol^{-1} and 11.1 kcal mol^{-1} from ***0s-im*** and ***0s-py***, respectively, resulting 5–1 kcal mol^{-1} higher than the analogous barriers for primary insertion (see Table S2 of the ESI†).

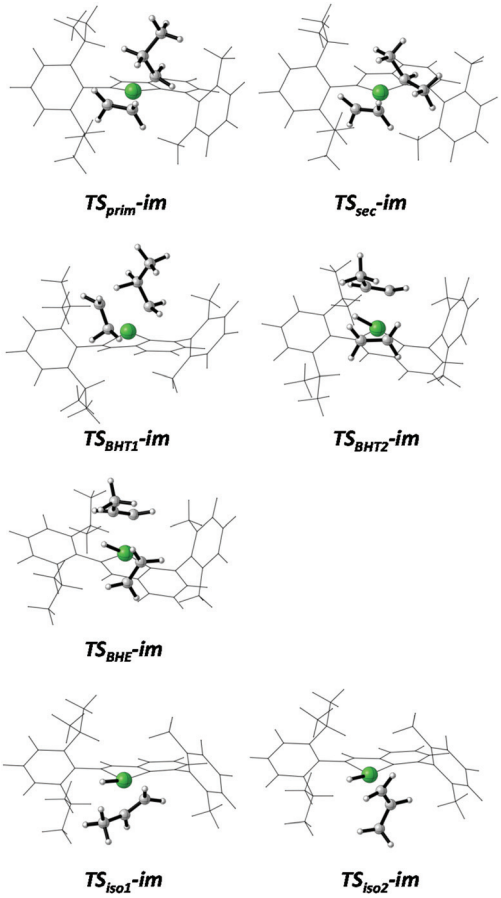

Fig. 5 Geometries of transition-state structures for ethylene insertion (***TS$_{prim}$-im***, ***TS$_{sec}$-im***), β-hydride transfer (***TS$_{BHT1}$-im***, ***TS$_{BHT2}$-im***), β-hydride elimination (***TS$_{BHE}$-im***) and for chain isomerization (***TS$_{iso1}$-im***, ***TS$_{iso2}$-im***).

The insertion barriers computed for the unsubstituted 2-(2,6-diisopropylphenyl)iminopyridine Ni(II) complex **2** are higher than those obtained for complex **1**: the barriers for primary insertion are 10.8 and 12.2 kcal mol^{-1} for the imine and pyridine isomers, and reasonably reflect the greater stability of the π-ethylene complexes. While this finding could appear in contrast with the experimentally observed similar activities of the two catalytic systems, the higher insertion barriers for catalyst **2** are balanced by the more favoured ethylene uptake, leading to a higher concentration of the ethylene alkyl complex, and consequently, to a faster propagation reaction.

Chain transfer. As mentioned in the introduction, it is well established that the presence of bulky groups in the two axial sites of the square coordination plane of diimine Ni(II) complexes is a required feature to obtain high molecular weight polyethylene, since it slows down the chain transfer rate *vs.* the rate of propagation.[1–9] Cavallo *et al.* proposed the use of topographic steric maps to visualize the catalytic pockets of these and other catalysts and to address the steric hindrance of the substituents on the ligand skeleton.[37] Thus, we traced the maps reporting the altimetry isocontour lines delimitating the encumbered zones of the ligand in the proximity of the active sites of catalyst **1**, and, for comparison, the analogous maps for the unsubstituted iminopyridine complex **2** and for the prototypical *N*,*N*′-(2,6-diisopropylphenyl)ethylenediimine Ni(II) Brookhart catalyst. For all the complexes, the metal atoms are placed at the centre of the maps and the complexes are oriented with the imine–pyridine or diimine metallacycle in the equatorial belt of the maps. As expected, the catalytic pocket produced by the *N*,*N*′-(2,6-diisopropylphenyl)ethylenediimine ligand consists of horizontal groove in the square planar coordination plane with four bulges at the periphery (Fig. 6a). It is evident how the four isopropyl *ortho* substituents encumber the axial coordination sites. In the steric map of complex **2**, the flat ligand principally occupies the space in the equatorial belt with small bulges in the NW and SW quadrants (Fig. 6b). The catalytic pocket sharpened by this ligand is substantially opened with free access to the axial coordination sites from the eastern hemisphere. In the steric map of complex **1**, the *ortho*-2,6-dimethylphenyl substituent of the pyridine moiety increases the space occupation of the ligand, with a major bulge protruding out of the plane containing the

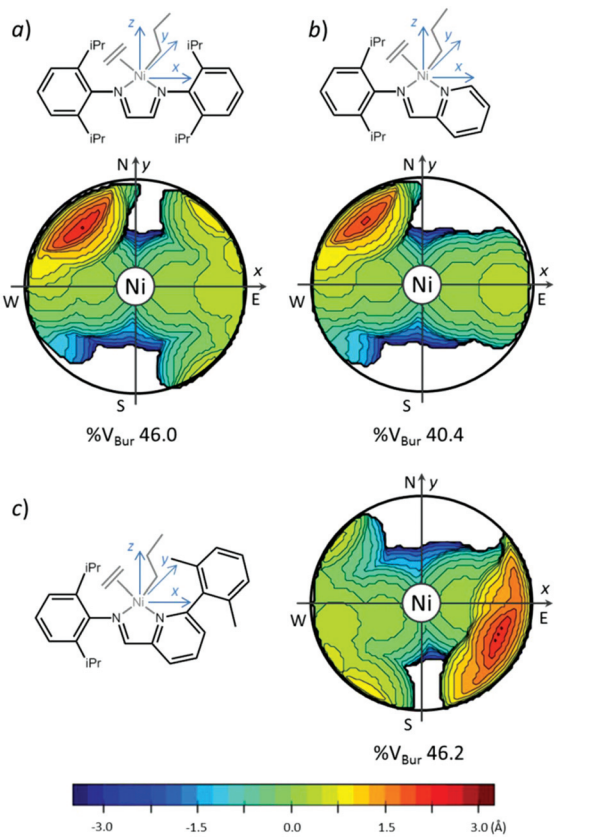

Fig. 6 Steric maps and percent buried volume (%V_{Bur}) of nickel(II) complexes featuring either *N*,*N*′-(2,6-diisopropyl-phenyl)ethylenediimine (a), or 6-(2,6-diisopropylphenyl)-2-iminopyridine ligand **L2** (b) or 6-(2,6-dimethylphenyl)-2-(2,6-diisopropylphenyl)iminopyridine **L1** (c) ligands. The isocontour curves are given in Å.

metal in the SE quadrant (Fig. 6c). As can be inferred by the steric map, only the southern axial site is sterically restricted whilst the northern axial site remains open. So, the catalytic pocket sharpened by the ligand is not effective in blocking both axial coordination site and it is not expected that chain propagation is favoured over chain transfer.

Subsequently, we turned to calculate the energetics of the termination processes, *i.e.* the β-H elimination (BHE) and the β-H transfer to the monomer (BHT). For the β-H elimination process, two distinct pathways have been proposed in the literature:[38] a dissociative displacement in which the olefinic chain produced by β-H elimination dissociates before the coordination of ethylene to the hydride complex and an associative displacement in which the dissociation of the olefinic chain occurs after the coordination of ethylene to the hydride complex. We computed the barrier height (TS_{BHE}) only for the associative displacement path, while we were not able to locate a stable tricoordinate hydride intermediate for the dissociative displacement path, similarly to previous DFT studies on ethylene polymerization promoted by α-diimine Ni(II) catalysts.[9,39] For β-H transfer to the monomer, two transition states have been identified in the literature differing for the position of the hydrogen atom that moves from the alkyl group to the coordinated monomer.[40,41] The hydrogen atom can be found far from the metal centre (TS_{BHT1}) or close to the metal centre (TS_{BHT2}), the latter case being characterized by a strong metal–hydrogen interaction.

All the transition states ***TS*$_{BHE}$-im**, ***TS*$_{BHE}$-py**, ***TS*$_{BHT1}$-im**, ***TS*$_{BHT1}$-py**, ***TS*$_{BHT2}$-im** and ***TS*$_{BHT2}$-py**, for the two distinct isomers of complex **1**, were located and the energy profiles for the termination process starting from the olefin π-intermediates **1-im** and **1-py** are reported in Fig. 4 (blue paths).

The position of the alkyl chain, *i.e. trans* to the imine ("imine" reaction path) or *trans* to the pyridine ("pyridine" reaction path) has little influence on the barrier heights: analogous transition states (*e.g.* ***TS*$_{BHT1}$-im** and ***TS*$_{BHT1}$-py**) in the two paths have similar barriers. The lowest barrier was obtained for the ***TS*$_{BHE}$**, so β-hydride elimination is expected to be the preferred termination reaction. In the BHT termination process, the assistance of the metal reduces the activation energy yielding ***TS*$_{BHT2}$** more viable than ***TS*$_{BHT1}$**. The optimized structure of ***TS*$_{BHE}$-im** is depicted in Fig. 5, where the structures of ***TS*$_{BHT1}$-im** and ***TS*$_{BHT2}$-im** are also displayed for comparison. The principal geometric difference between ***TS*$_{BHT2}$-im** and ***TS*$_{BHE}$-im** is the orientation of the coordinated ethylene, which is parallel to the Ni–H bond in the case of ***TS*$_{BHT2}$-im** and orthogonal to the Ni–H bond in the case of ***TS*$_{BHE}$-im**.

The difference between the activation barriers of the termination reaction and chain propagation ($\Delta G^{\ddagger}_{BHE-CP}$) provides an estimation of the oligomerization degree for the catalytic cycle. The difference we obtained are 8.9 and 7.1 kcal mol^{-1}, for the imine and pyridine reaction paths, respectively. These values are quite low and are consistent with the low molecular weight polyethylene obtained by catalyst **1**. For comparison, $\Delta G^{\ddagger}_{BHE-CP}$ values were also computed for the unsubstituted iminopyridine complex **2** and for *N*,*N*′-(2,6-diisopropylphenyl) ethylenediimine nickel(II) complex, the energy profiles corresponding to the propagation and termination reactions are reported in ESI.† In the case of complex **2**, the $\Delta G^{\ddagger}_{BHE-CP}$ values were slightly lower than those obtained for complex **1**: 5.5 and 8.2 kcal mol^{-1}, for the imine and pyridine reaction paths, respectively. Both catalytic systems experimentally provide low molecular weight polyethylene. In the case of Brookhart's *N*,*N*′-(2,6-diisopropylphenyl)ethylenediimine nickel(II) complex, which is known to produce high molecular weight polyethylene, the $\Delta G^{\ddagger}_{BHE-CP}$ value was 10.8 kcal mol^{-1}, in agreement with the experimental results.

Chain isomerization reactions. It is generally accepted that the chain branching originates from a chain isomerization of the primary alkyl agostic complex during the polymerization process.[7] A β-hydride elimination from the primary alkyl complex leads to an olefin hydride intermediate that, after rotation of the π-coordinated olefin, produces a secondary alkyl complex. Ethylene trapping and subsequent insertions yields a methyl branch in the polymer chain. Further isomerization of the secondary alkyl complex (without monomer trapping) results in the "chain walking" along the polymer chain and the production of long chain branches.

The reaction paths for the "primary to secondary alkyl" isomerization for complex **1** are reported in Fig. 4 (red paths). In the first step, the formation of the hydride intermediate has a barrier of either 15.6 kcal mol^{-1} or 15.3 kcal mol^{-1} for the imine or the pyridine reaction path, respectively. In these intermediates (***H-im*** and ***H-py***) the olefin is orthogonal to the plane of the metallacycle as typical for out-of-the-plane π complexes. The step is endoergonic but further rotation of the olefin has a very small activation barrier, 1.1 kcal mol^{-1} or 0.2 kcal mol^{-1} with respect to the hydride intermediate for the "imine" or "pyridine" reaction path, respectively. The isomerization from primary to secondary alkyl is practically isoergonic for both reaction paths. These DFT results point out that the isomerization process is easily viable and competitive over propagation.

However, it is worth noting that the degree of branching and the topology of the polymers have been justified using stochastic simulations since it is not simple to predict the microstructure on the basis of the DFT calculations.[42,43] In fact, they depend on various factors, often contrasting with each other, such as: (i) the relative stabilities of the primary *vs.* secondary alkyl complexes; (ii) the relative stability of the primary *vs.* secondary alkyl-ethylene π-complexes; (iii) the differences of the barriers for the "primary" and "secondary" insertions; (iv) the competition between isomerization of the alkyl complexes and ethylene trapping.

However, the above DFT results can shed light on the different behaviour of complexes **1** and **2** with respect to the branching density of the produced polyethylenes. By comparing the free energy profiles corresponding to the different reaction paths for the two catalysts, it results that the major difference lies in the free energy variation due to ethylene uptake of the alkyl complexes, which is 6.8–9.0 kcal mol^{-1} for **1** and

2.9–1.3 kcal mol^{-1} for **2**. This implies that coordination of ethylene to form the alkyl π-olefin is more probable for **2** than for **1**, resulting in easier chain propagation and thus in the production of a polyethylenes with a lower branching density.

Conclusions

A Ni(II) complex bearing an asymmetrical iminopyridine ligand, featuring a 2,6-dimethylphenyl substituent in the *ortho* position of the pyridine moiety and a 2,6-diisopropylphenyl substituent on the imine nitrogen, was synthesized, structurally characterized and tested in the polymerization of ethylene after activation with $AlEt_2Cl$. Unexpectedly, hyperbranched low molecular weight polyethylene oils were produced under a variety of reaction conditions. The content of "branches on branch", indicated by the presence of *sec*-butyl branches, increases while decreasing the monomer pressure, as previously observed for α-diimine Pd catalysts. The DFT calculations showed that the polymerization behaviour of **1** can be addressed to the catalytic pocket generated by the coordinated ligand. Specifically, the *ortho*-2,6-dimethylphenyl substituent of the pyridine group hinders the coordination sites destabilizing the ethylene coordination but, at the same time, it is oriented in such a way that does not encumber both axial coordination sites. This has the consequence that both chain transfer and chain walking are favoured over propagation.

The hyperbranched low viscosity oligoethylene oils reported above may have interesting applications as synthetic base stocks in the formulation of high performance synthetic lubricants, as suggested for similar materials produced by Pd catalysts,[13] and the possible use of less expensive Ni catalysts could stimulate the development of such processes.

Experimental section

General procedures

All manipulations involving air and/or moisture-sensitive compounds were performed under an atmosphere of nitrogen in a Braun Labmaster glovebox or using Schlenk techniques. Glassware used were dried in an oven at 120 °C overnight and exposed three times to vacuum–nitrogen cycles. Toluene and *o*-dichlorobenzene were refluxed over metallic sodium, dichloromethane was refluxed over CaH_2 and hexane was refluxed over sodium-benzophenone. They were distilled under nitrogen before use. Deuterated solvents were purchased from Aldrich and stored in the glovebox over 3 Å molecular sieves before use. All other reagents were purchased from Aldrich and used as received. Ethylene was purchased from SON and used without further purification.

The NMR spectra were recorded on a Bruker Advance 400 and a Bruker 600 MHz Ascend 3 HD spectrometers. Chemical shifts (δ) are expressed as parts per million. ^{1}H NMR spectra are referenced using the residual solvent peak at δ 7.26 for $CDCl_3$ and δ 5.32 for CD_2Cl_2. ^{13}C NMR spectra are referenced using the residual solvent peak at δ 77.216 for $CDCl_3$ and δ 53.84 for CD_2Cl_2.

The molecular weights (M_n and M_w) and the molecular mass distribution (M_w/M_n) of the polymer samples were measured by gel permeation chromatography (GPC) at 30 °C, using THF as solvent, an eluent flow rate of 1 mL min^{-1}, and narrow polystyrene standards as reference. The measurements were performed on a Waters 1525 binary system equipped with a Waters 2414 RI detector using four Styragel columns (range 1000–1 000 000 Å).

High-resolution mass spectra (HRMS) were acquired by using a Bruker solariX XR Fourier transform ion cyclotron resonance mass spectrometer (Bruker Daltonik GmbH, Bremen, Germany) equipped with a 7T refrigerated actively-shielded superconducting magnet (Bruker Biospin, Wissembourg, France). The samples were ionized in positive ion mode by using the ESI ion source (Bruker Daltonik GmbH, Bremen, Germany). The mass range was set to m/z 150–3000. The mass spectra were calibrated externally by using a NaTFA solution in positive-ion mode. A linear calibration was applied.

Volatile unsaturated oligomers were analyzed by capillary chromatography using a GC7890A Agilent gas chromatograph equipped with a MSD5975 mass detector. Fused silica DB 17MS capillary column 30 m long, 0.25 mm I.D. 0.25 μm film thickness was used with a temperature-programmed run from 35 to 150 °C at a rate of 2 °C min^{-1}. The identification of unsaturated oligomers contents in the reaction mixture was confirmed by mass spectrometry data analysis and their quantification has been performed using hexane as internal standard and a selected ion monitoring (SIM) acquisition mode as method to increase the detector sensitivity.

Syntheses and characterizations of the ligand (L1) and of the nickel complex 1

Ligand **L1** and complex **1** were synthesized adapting literature procedures.[44,45]

6-Bromo-2-(2,6-diisopropylphenyl)iminopyridine (A). 2-Formyl-6-bromopyridine (7.12 g, 38 mmol) and 2,6-diisopropylaniline (6.79 g, 38 mmol) were dissolved in 120 mL of anhydrous toluene containing 0.3 nm pare size molecular sieves (3 g) and 8 mg of *p*-TsOH. The mixture was heated to 70° C under N_2 for 16 h. After filtration and removal of the volatiles under reduced pressure, a yellow solid was isolated, (13 g, 99% yield). ESI(+)-MS analysis:[344.09]; (MH^+) 345.09, 347.09; (MNa^+) 367.08, 369.08.

^{1}H NMR ($CDCl_3$, 400 MHz, 25 °C): δ 8.27 (d, J = 7.6 Hz, $1H_{pyridine}$), 8.25 (s, 1H, –HC═N–), 7.69 (t, J = 7.6 Hz, $1H_{pyridine}$), 7.61 (d, J = 7.6 Hz, $1H_{pyridine}$), 7.26–7.12 (m, $3H_{aryl}$), 2.92 (sept, J = 6.8 Hz, 2H, $CH(CH_3)_2$), 1.17 (d, J = 6.8 Hz, 12H, $CH(CH_3)_2$). ^{13}C NMR ($CDCl_3$, 100.67 MHz, 25 °C): δ 161.63 (–CH═N–), 155.62 (C), 148.05 (C), 142.00 (C), 139.15 (CH), 137.18 (CH), 129.96 (CH), 124.84 (2C), 123.22 (2CH), 120.03 (CH), 28.10 ($CH(CH_3)_2$), 22.59 ($CH(CH_3)_2$).

6-(2,6-Dimethylphenyl)-2-(2,6-diisopropylphenyl)iminopyridine (L1). To a suspension of 6-bromo-2-(2,6-diisopropylphenyl) iminopyridine (2.76 g, 8.00 mmol) and $Pd(PPh_3)_4$ (0.25 g,

0.22 mmol) in toluene (20 mL), aqueous 2.0 M Na_2CO_3 (10 mL) and 2,6-dimethylphenylboronic acid (1.80 g, 12.00 mmol) dissolved in methanol (8 mL) were subsequently added. After refluxing the suspension for 16 h, a 2.0 M aqueous solution of Na_2CO_3 (50 mL) and CH_2Cl_2 (100 mL) were added to the solution after cooling to room temperature. The aqueous phase was separated and extracted with CH_2Cl_2 (30 mL), and the combined organic extracts were dried using Na_2SO_4. Further purification by a silica gel column chromatography, using 9 : 1 hexane/ethyl acetate as the eluent, gave the title compounds as a pale yellow solid (1.40 g, 47% yield). HRMS (ESI+) *m*/*z* calcd for $C_{26}H_{30}N_2$: [370.2409]; found: 371.2484 $[L1–H]^+$; 393.2304 $[L1–Na]^+$. ^1H NMR (400 MHz, CD_2Cl_2, 25 °C): δ = 8.36 (s, 1 H, –N=CH–), 8.24 (d, J = 7.6 Hz, $1H_{pyridine}$), 7.96 (t, J = 7.6 Hz, $1H_{pyridine}$), 7.38 (d, J = 7.6, $1H_{pyridine}$), 7.20–7.13 (m, $6H_{aryle}$), 3.00 [sept, J = 6.8 Hz, 2H, $CH(CH_3)_2$], 2.08 (s, 6H, CH_3), 1.17 [d, J = 6.8 Hz, 12H, $CH(CH_3)_2$]. ^{13}C NMR (100.67 MHz, CD_2Cl_2, 25 °C): δ = 163.29 (–N=CH–), 159.76 (C), 154.31 (C), 148.35 (C), 139.73 (C), 137.13 (2C), 137.01 (CH), 135.84 (2C), 128.17 (CH), 127.79 (2CH), 126.21 (CH), 124.35 (CH), 122.96 (2CH), 119.08 (CH), 27.90 [$CH(CH_3)_2$], 23.41 [$CH(CH_3)_2$], 20.34 (CH_3).

6-(2,6-Dimethylphenyl)-2-(2,6-diisopropylphenyl) iminopyridine nickel(II) dibromide (1). Compound **L1** (0.186 g, 0.51 mmol) and [$NiBr_2$(dme)] (0.152 g, 0.49 mmol), were dissolved in CH_2Cl_2 (40 mL) in a Schlenk flask under an atmosphere of nitrogen. The reaction mixture was stirred a room temperature for 24 h. The solvent was removed under vacuum and the red residue washed with dry hexane. The product was crystallized from dichloromethane/hexane (0.258 g, 86% yield). HRMS (ESI+) *m*/*z* calcd for $C_{26}H_{30}Br_2NiN_2$: 586.0120; found: 507.0943 $[L1–Ni–Br]^+$.

General procedure for ethylene oligomerization at 1 atm

Ethylene oligomerizations at 1 atm were all carried out in a glass reactor (100 cm^3) equipped with a mechanical stirrer and a temperature probe. In a typical run, under nitrogen atmosphere, the reactor vessel was charged with 25 ml of toluene, pressurized to 1 atm of ethylene and vented three times. Under ethylene atmosphere, the stirred mixture was thermostated at the required temperature and then a toluene solution of cocatalyst and a *o*-dichlorobenzene solution of catalyst were added sequentially. After the prescribed time, a sample of the reaction mixture was taken to be analysed *via* GC-MS and quantify the soluble products. Then the mixture was vented and poured into acidified methanol. Oligomers were extracted with hexane, dried on $MgSO_4$, filtered and dried under reduced pressure overnight at 80 °C.

General procedure for ethylene oligomerization at high ethylene pressures

Ethylene oligomerizations at high ethylene pressure (5–50 atm) were all carried out in a Büchi glass autoclave for polymerization at 5 atm of ethylene and in a stainless steel high pressure reactor for ethylene pressure 15–50 atm. The reactor was first dried overnight at 120 °C in an oven, cooled under vacuum, then pressurized with ethylene and vented using 3 cycles. Under vacuum, the reactor was thermostated at the require temperature, charged with toluene solution of cocatalyst and catalyst (50 ml) and then pressured to the prescribed ethylene pressure. Analysis and work up of the reaction mixtures were carried out as described above for the runs at 1 atm.

X-ray crystallographic studies

X-ray diffraction data were collected at the X-ray diffraction beamline (XRD1) of the Elettra Synchrotron of Trieste (Italy), with a Pilatus 2M image plate detector. Collection temperature was 100 K (nitrogen stream supplied through an Oxford Cryostream 700); the wavelength of the monochromatic X-ray beam was 0.700 Å and the diffractograms were obtained with the rotating crystal method. The crystals were dipped in *N*-paratone and mounted on the goniometer head with a nylon loop. The diffraction data were indexed, integrated and scaled using XDS.[46] Two independent collections for two different crystals were merged together in order to increase completeness.

The structure was solved by the dual space algorithm implemented in the SHELXT code.[47] Fourier analysis and refinement were performed by the full-matrix least-squares methods based on F^2 implemented in SHELXL.[48] The Coot program was used for modelling.[49] Anisotropic thermal motion was allowed for all non-hydrogen atoms. Hydrogen atoms were placed at calculated positions with isotropic factors $U = 1.2 \times U_{eq}$, U_{eq} being the equivalent isotropic thermal factor of the bonded non hydrogen atom. A CH_2Cl_2 solvent molecule was sitting near an inversion centre and was found to be disordered over three distinct positions: the corresponding three populations (summing to 0.5 due to the vicinity of the inversion centre) were refined to 0.32, 0.14 and 0.04 (selected quantitative information regarding data reduction and refinement is gathered in Table 5).

Computational details

Density functional theory (DFT) calculations were performed with the program suite Gaussian 09.[50] All geometries were optimized without constraints at the BP86 level, *i.e.*, employing the exchange and correlation functionals of Becke and Perdew, respectively.[51–53] The basis set employed was the LANL2DZ with associate effective core potentials for Ni[54] and 6-31G(d) for O, N, C, and H. Stationary point geometries were characterized as local minimum on the potential energy surfaces. The absence of imaginary frequency verified that structures were true minima at their respective levels of theory. The structures of transition state were located by applying Schlegel's synchronous-transit-guided quasi-Newton (QST2) method as implemented in GAUSSIAN 09. The transition states were verified with frequency calculations to ensure they were first order saddle points with only one negative eigenvalue. For the β-H elimination transition states, calculation of intrinsic reaction coordinates (IRC)[55–57] was conducted to unambiguously verify the connection between the right reactant and product. The buried volume calculations were performed with the SambVca

Table 5 Essential X-ray diffraction and refinement data for complex **1**

Formula	$C_{26}H_{30}Br_2N_2Ni\cdot\frac{1}{2}CH_2Cl_2$
Molar mass (Da)	631.51
Temperature (K)	100 (2)
Wavelength (Å)	0.700
Crystal system	Monoclinic
Space group	*P*21/*c*
a (Å)	14.210 (6)
b (Å)	14.561 (1)
c (Å)	14.996 (2)
α (°)	90
β (°)	110.079 (6)
γ (°)	90
V (Å^3)	2914 (1)
Z	4
ρ (g cm^{-3})	1.439
$F_{(000)}$	1276
μ (mm^{-1})	3.382
θ min, max (°)	1.503, 24.941
Resolution (Å)	0.83
Total refl. collected	65 998
Independent refl.	5145
Obs. refl. ($F_o > 4\sigma F_o$)	4696
I/σ_I (all data)	73.45
I/σ_I (max resltn)	29.85
R_{merge} (all data)	2.3%
R_{merge} (max resltn)	7.8%
Completeness (all data)	0.965
Completeness (max resltn)	0.964
Multiplicity (all data)	12.6
Multiplicity (max resltn)	13.1
Data/restraint/parameters	5145/12/284
$R_{I>2\sigma_I}$, w$R_{I>2\sigma_I}$	0.0399, 0.1078
R (all data), wR_2 (all data)	0.0442, 0.1127
GooF	1.036

package, a software free of charge developed by Cavallo *et al.*[37] The radius of the sphere around the metal centre was set to 3.5 Å, while for the atoms we adopted the Bondi radii scaled by 1.17, and a mesh of 0.1 Å was used to scan the sphere for buried voxels. The steric maps were evaluated with a development version of the SambVca package.

Cartesian coordinates of all DFT optimized structures are available on request. Structures were visualized by the CYLview program.[58]

Conflicts of interest

There are no conflicts to declare.

Acknowledgements

The authors thank Dr Patrizia Oliva for NMR assistance, Dr Patrizia Iannece for Mass spectrometry analyses and Stefano Caputo for performing some polymerization runs.

Notes and references

1 L. K. Johnson, C. M. Killian and M. Brookhart, *J. Am. Chem. Soc.*, 1995, **117**, 6414–6415.
2 Reviews: S. D. Ittel, L. K. Johnson and M. Brookhart, *Chem. Rev.*, 2000, **100**, 1169–1203.
3 V. C. Gibson and S. K. Spitzmesser, *Chem. Rev.*, 2003, **103**, 283–316.
4 M. Delferro and T. J. Marks, *Chem. Rev.*, 2011, **111**, 2450–2485.
5 W.-H. Sun, *Adv. Polym. Sci.*, 2013, **258**, 163–178.
6 H. Mu, L. Pan, D. Song and Y. Li, *Chem. Rev.*, 2015, **115**, 12091–12137.
7 L. Guo, S. Dai, X. Sui and C. Chen, *ACS Catal.*, 2016, **6**, 428–441.
8 D. P. Gates, S. A. Svejda, E. Oñate, C. M. Killian, L. K. Johnson, P. S. White and M. Brookhart, *Macromolecules*, 2000, **33**, 2320–2334.
9 L. Deng, T. K. Woo, L. Cavallo, P. M. Margl and T. Ziegler, *J. Am. Chem. Soc.*, 1997, **119**, 6177–6186.
10 Z. Guan, P. M. Cotts, E. F. McCord and S. J. McLain, *Science*, 2000, **283**, 2059–2062.
11 P. M. Cotts, Z. Guan, E. McCord and S. McLain, *Macromolecules*, 2000, **33**, 6965–6969.
12 S. A. Svejda and M. Brookhart, *Organometallics*, 1999, **18**, 65–74.
13 P. Xiang, Z. Ye and R. Subramanian, *Polymer*, 2011, **52**, 5027–5039.
14 Recent reviews: Z. Dong and Z. Ye, *Polym. Chem.*, 2012, **3**, 286–301.
15 Y. Chen, L. Wang, H. Yu, Y. Zhao, R. Sun, G. Jing, J. Huang, H. Khalid, N. M. Abbasi and M. Akram, *Prog. Polym. Sci.*, 2015, **45**, 23–43.
16 B. I. Voit and A. Lederer, *Chem. Rev.*, 2009, **109**, 5924–5973.
17 M. A. Zuideveld, P. Wehrmann, C. Röhr and S. Mecking, *Angew. Chem., Int. Ed.*, 2004, **43**, 869–873.
18 T. Wiedemann, G. Voit, A. Tchernook, P. Roesle, I. Götter-Schnetmann and S. Mecking, *J. Am. Chem. Soc.*, 2014, **136**, 2078–2085.
19 C. J. Stephenson, J. P. McInnis, C. Chen, M. P. Weberski, A. Motta, M. Delferro and T. J. Marks, *ACS Catal.*, 2014, **4**, 999–1003.
20 D. Zhang, E. T. Nadres, M. Brookhart and O. Daugulis, *Organometallics*, 2013, **32**, 5136–5143.
21 T. V. Laine, M. Klinga and M. Leskelä, *Eur. J. Inorg. Chem.*, 1999, **1999**, 959–964.
22 T. V. Laine, K. Lappalainen, J. Liimatta, E. Aitola, B. Löfgren and M. Leskelä, *Macromol. Rapid Commun.*, 1999, **20**, 487–491.
23 T. V. Laine, U. Piironen, K. Lappalainen, M. Klinga, E. Aitola and M. Leskelä, *J. Organomet. Chem.*, 2000, **606**, 112–124.
24 T. Irrgang, S. Keller, H. Maisel, W. Kretschmer and R. Kempe, *Eur. J. Inorg. Chem.*, 2007, **2007**, 4221–4228.
25 W.-H. Sun, S. Song, B. Li, C. Redshaw, X. Hao, Y.-S. Li and F. Wang, *Dalton Trans.*, 2012, **41**, 11999–12010.
26 E. Yue, L. Zhang, Q. Xing, X.-P. Cao, X. Hao, C. Redshaw and W.-H. Sun, *Dalton Trans.*, 2014, **43**, 423–431.
27 E. Yue, Q. Xing, L. Zhang, Q. Shi, X.-P. Cao, L. Wang, C. Redshaw and W.-H. Sun, *Dalton Trans.*, 2014, **43**, 3339–3346.

28 Z. Chen, K. E. Allen, P. S. White, O. Daugulis and M. Brookhart, *Organometallics*, 2016, **35**, 1756–1760.

29 S. Song, Y. Li, C. Redshaw, F. Wang and W.-H. Sun, *J. Organomet. Chem.*, 2011, **696**, 3772–3778.

30 K. Nienkemper, V. V. Kotov, G. Kehr, G. Erker and R. Frohlich, *Eur. J. Inorg. Chem.*, 2006, **2006**, 366–379.

31 D. Pappalardo, M. Mazzeo and C. Pellecchia, *Macromol. Rapid Commun.*, 1997, **18**, 1017–1023.

32 P. M. Cotts, Z. Guan, E. McCord and S. McLain, *Macromolecules*, 2000, **33**, 6945–6952.

33 G. B. Galland, R. F. deSouza, R. S. Mauler and F. F. Nunes, *Macromolecules*, 1999, **32**, 1620–1625.

34 Y. Zhang, C. Huang, X. Wang, Q. Mahmood, X. Hao, X. Hu, C.-Y. Guo, G. A. Solan and W.-H. Sun, *Polym. Chem.*, 2017, **8**, 995–1005.

35 T. K. Woo, P. E. Blöchl and T. Ziegler, *J. Phys. Chem. A*, 2000, **104**, 121–129.

36 The ethylene insertion and the chain transfer mechanisms of the 2-(2,6-diisopropylphenyl)iminopyridine nichel(II) complex was already investigated: J. Ramosa, V. Cruz, A. Muñoz-Escalona, S. Martínez and J. Martínez-Salazar, *Polymer*, 2003, **44**, 2169–2176.

37 L. Falivene, R. Credendino, A. Poater, A. Petta, L. Serra, R. Oliva, V. Scarano and L. Cavallo, *Organometallics*, 2016, **35**, 2286–2293.

38 W. Heyndrickx, G. Occhipinti and V. R. Jensen, *Chem. – Eur. J.*, 2014, **20**, 7962–7978.

39 L. Deng, P. Margl and T. Ziegler, *J. Am. Chem. Soc.*, 1997, **119**, 1094–1100.

40 G. Talarico and P. H. M. Budzelaar, *J. Am. Chem. Soc.*, 2006, **128**, 4524–4525.

41 G. Talarico and P. H. M. Budzelaar, *Organometallics*, 2008, **27**, 4098–4107.

42 A. Michalak and T. Ziegler, *J. Am. Chem. Soc.*, 2002, **124**, 7519–7528.

43 A. Michalak and T. Ziegler, *Organometallics*, 2003, **22**, 2069–2079.

44 K. A. Frazier, R. D. Froese, Y. He, J. Klosin, C. N. Theriault, P. C. Vosejpka and Z. Zhou, *Organometallics*, 2011, **30**, 3318–3329.

45 T. Arai and K. Suzuki, *Synlett*, 2009, 3167–3170.

46 W. Kabsch, *Acta Crystallogr., Sect. D: Biol. Crystallogr.*, 2010, **66**, 125–132.

47 G. M. Sheldrick, *Acta Crystallogr., Sect. A: Fundam. Crystallogr.*, 2015, **71**, 3–8.

48 G. M. Sheldrick, *Acta Crystallogr., Sect. A: Fundam. Crystallogr.*, 2008, **64**, 112–122.

49 P. Emsley and K. Cowtan, *Acta Crystallogr., Sect. D: Biol. Crystallogr.*, 2004, **60**, 2126–2132.

50 M. J. Frisch, G. W. Trucks, H. B. Schlegel, G. E. Scuseria, M. A. Robb, J. R. Cheeseman, G. Scalmani, V. Barone, B. Mennucci, G. A. Petersson, H. Nakatsuji, M. Caricato, X. Li, H. P. Hratchian, A. F. Izmaylov, J. Bloino, G. Zheng, J. L. Sonnenberg, M. Hada, M. Ehara, K. Toyota, R. Fukuda, J. Hasegawa, M. Ishida, T. Nakajima, Y. Honda, O. Kitao, H. Nakai, T. Vreven, J. A. Montgomery Jr., J. E. Peralta, F. Ogliaro, M. Bearpark, J. J. Heyd, E. Brothers, K. N. Kudin, V. N. Staroverov, R. Kobayashi, J. Normand, K. Raghavachari, A. Rendell, J. C. Burant, S. S. Iyengar, J. Tomasi, M. Cossi, N. Rega, J. M. Millam, M. Klene, J. E. Knox, J. B. Cross, V. Bakken, C. Adamo, J. Jaramillo, R. Gomperts, R. E. Stratmann, O. Yazyev, A. J. Austin, R. Cammi, C. Pomelli, J. W. Ochterski, R. L. Martin, K. Morokuma, V. G. Zakrzewski, G. A. Voth, P. Salvador, J. J. Dannenberg, S. Dapprich, A. D. Daniels, O. Farkas, J. B. Foresman, J. V. Ortiz, J. Cioslowski and D. J. Fox, *Gaussian 09, revision A.02*, Gaussian, Inc., Wallingford, CT, 2009.

51 A. D. Becke, *Phys. Rev. A*, 1988, **38**, 3098–3100.

52 J. P. Perdew, *Phys. Rev. B: Condens. Matter*, 1986, **33**, 8822–8824.

53 J. P. Perdew, *Phys. Rev. B: Condens. Matter*, 1986, **34**, 7406–7406.

54 P. J. Hay and W. R. Wadt, *J. Chem. Phys.*, 1985, **82**, 270–283.

55 K. Fukui, *Acc. Chem. Res.*, 1981, **14**, 363–368.

56 C. Gonzalez and H. B. Schlegel, *J. Chem. Phys.*, 1989, **90**, 2154–2161.

57 C. Gonzalez and H. B. Schlegel, *J. Chem. Phys.*, 1990, **94**, 5523–5527.

58 C. Y. Legault, *CYLview, v1.0b*, Université de Sherbrooke, 2009; http://www.cylview.org.